DOI: 10.22226/2410-3535-2018-3-311-316 PACS: 62.20.fq, 61.72.-y, 62.20.F-, 61.66.Dk

Onset of plastic deformation in non-equiatomic fcc CoCrFeMnNi high-entropy alloys under high-rate loading

A. V. Korchuganov†

†avkor@ispms.ru

Institute of Strength Physics and Materials Science, Siberian Branch of RAS, 2/4 Akademicheskiy ave., Tomsk, 634055, Russia

Based on molecular dynamics computer simulations, features of the nucleation and evolution of plastic deformation under high-rate mechanical loading of CoCrFeMnNi high-entropy alloy single crystals with different stoichiometric compositions were studied. To obtain a thermodynamically equilibrium distribution of chemical elements, the relaxation of samples was carried out using the Monte Carlo method. Calculations showed that an increase in the fraction of Co and Ni, or a decrease in the fraction of Cr, Fe, and Mn led to an increase in the Young's modulus of the alloy. Based on these calculations, two samples with different stoichiometric compositions were selected and investigated: $Co_{30}Cr_{30}Fe_{10}Mn_{10}Ni_{20}$ ($Co_{30}Cr_{30}$-sample) and $Co_{10}Cr_{10}Fe_{30}Mn_{30}Ni_{20}$ ($Fe_{30}Mn_{30}$-sample) with high and low Young's moduli, respectively. A comparison was also made with the equiatomic alloy. Regardless of composition, the onset of plasticity in CoCrFeMnNi single crystals is realized through the formation and growth of intrinsic stacking faults and bands with an hcp lattice. The mechanism for their formation is the rearrangement of the lattice from fcc to bcc and then to an hcp structure. Structural and mechanical responses of the samples differ substantially for different alloy compositions, types and rates of mechanical loading. The nucleation and growth of stacking faults and hcp-phase layers are suppressed in the $Co_{30}Cr_{30}$-sample, and consequently, its elastic limit stresses are more than twice higher than the respective values for the $Fe_{30}Mn_{30}$-sample. After the formation of these defects, twinning takes place under tension in all samples, but it is not observed under compression. The plasticity mechanisms of high-entropy alloys and fcc nickel are in many respects similar. The obtained results enabled establishing a relationship between the stoichiometric composition and the atomic mechanisms of plastic deformation of high-entropy alloys under various types of mechanical loading.

Keywords: high-entropy alloys, stoichiometric composition, plastic deformation, molecular dynamics, stacking faults.

УДК: 539.214, 539.4, 54 – 165.2, 539.213

Зарождение пластической деформации в высокоэнтропийных ГЦК сплавах CoCrFeMnNi неэквиатомного состава при высокоскоростном нагружении

Корчуганов А. В.†

Институт физики прочности и материаловедения СО РАН, пр. Академический 2/4, Томск, 634055, Россия

На основе компьютерного моделирования методом молекулярной динамики исследованы особенности зарождения и развития пластической деформации при высокоскоростном механическом нагружении монокристаллов высокоэнтропийного сплава CoCrFeMnNi с различным стехиометрическим составом. Чтобы получить термодинамически равновесное распределение химических элементов, релаксация образцов проводилась с использованием метода Монте-Карло. Расчеты показали, что увеличение доли Co и Ni или уменьшение доли Cr, Fe и Mn приводит к увеличению модуля Юнга сплава. На основе этих расчетов были выбраны и исследованы два образца различного стехиометрического состава: $Co_{30}Cr_{30}Fe_{10}Mn_{10}Ni_{20}$ ($Co_{30}Cr_{30}$-образец) и $Co_{10}Cr_{10}Fe_{30}Mn_{30}Ni_{20}$ ($Fe_{30}Mn_{30}$-образец), с высоким и низким модулем Юнга, соответственно. Также было проведено сравнение с эквиатомным сплавом. Независимо от состава зарождение пластичности в монокристаллах CoCrFeMnNi реализуется посредством образования и роста дефектов упаковки вычитания и полос с ГПУ решеткой. Механизмом их формирования является перестройка решетки из ГЦК в ОЦК и затем в ГПУ структуру. Структурный и механический отклик образцов существенно раз-

личается для разных составов сплава, типов и скоростей механической нагрузки. Зарождение и рост дефектов упаковки и прослоек ГПУ фазы подавлены в $Co_{30}Cr_{30}$-образце, вследствие чего напряжения предела упругости в нем более чем в два раза больше значений для $Fe_{30}Mn_{30}$-образца. Во всех образцах после образования этих дефектов при растяжении происходит двойникование. При сжатии его не наблюдается. Механизмы пластичности ВЭС и ГЦК никеля во многом схожи. Полученные результаты позволили установить связь между стехиометрическим составом и атомными механизмами пластической деформации высокоэнтропийных сплавов при различных видах механического нагружения.

Ключевые слова: высокоэнтропийные сплавы, стехиометрический состав, пластическая деформация, молекулярная динамика, дефекты упаковки.

1. Introduction

Study of the structure and behavior of high-entropy alloys (HEAs) under thermal and mechanical actions is one of the most relevant topics of modern materials science [1], which is conditioned by their extraordinary physical and mechanical properties, in contrast to conventional alloys. For example, CoCrFeMnNi alloys are characterized by a high strength, ductility and crack resistance [2]. The $Co_{1.5}CrFeNi_{1.5}Ti_{0.5}Mo_{0.1}$ alloy has a high corrosion resistance and in terms of wear resistance is superior to conventional steels with a similar hardness [3].

Most often, HEAs with an equiatomic composition are investigated, because it is considered that they should be more thermodynamically stable due to the maximum configuration entropy [4]. At the same time, HEAs with a non-equiatomic composition also remain stable and often have even better properties [5]. Therefore, finding new stoichiometric compositions of HEAs is a topical task of materials science [6]. Alongside with labor-intensive and expensive experimental studies, computer simulation is an efficient tool which enables generating and processing quickly large amounts of information, and also determining the material's chemical composition corresponding to the required properties. For instance, on the basis of thermodynamic calculations in [7] over 130000 multi-component systems with potentially good mechanical properties were proposed.

At present, studies are actively conducted to reveal the mechanisms governing the behavior of HEAs under mechanical loads [8]. For example, the high strength of HEAs is attributed to the effects of solid-solution strengthening [9 – 10]. It was shown in [11] that the pinning of dislocations due to a severe distortion of the crystal lattice is the principal mechanism of plastic deformation for the $AlCrFeCuNi_{1.4}$ alloy. In [12], on the basis of molecular-dynamics and first-principles calculations, specific atomic rearrangements were discovered during the compression of AlCrCoFeNi crystallites, leading to chemical disordering and a reduction in the element segregation degree.

Today, the CoCrFeMnNi HEA is characterized by high physical and mechanical properties and has a great potential for their improvement [13 – 15]. The atomic mechanisms of the plastic deformation of this alloy, as well as the stoichiometric composition's effect on them, still remain unclarified to a large extent. To solve this task, the most effective way is computer simulation based on the method of molecular dynamics (MD). This method explicitly takes into account the material's atomic structure and enables studying the dynamics of structural transformations occurring therein under various types of external action [16,17]. Therefore, the aim of the present study is to reveal the effect of the stoichiometric composition on the atomic mechanisms of plastic deformation of the CoCrFeMnNi HEA in the framework of MD simulation.

2. Simulation procedure

The calculations were made in the LAMMPS software [18]. To describe the interatomic interaction in CoCrFeMnNi, many-body potentials [19,20] built in the framework of a modified embedded-atom method, taking into account the second nearest neighbors, were used. The applicability of the used interatomic potentials for the description of the properties of the HEA under study was substantiated in the paper [21] on the basis of the comparison between the MD simulation data, *ab-initio* calculations and experimental data.

During the relaxation of the samples, the MD method and the Monte Carlo method (the Metropolis algorithm) were used jointly in the calculations. In the framework of this approach, randomly selected atoms of various types exchange places (Monte Carlo steps) with a probability of $p = \min\{1, \exp[-\beta\Delta U]\}$, where ΔU is the change in the total energy of the system in the permutation, β is the temperature parameter, and the relaxation of the material's structure is done in the framework of the MD method [22].

The initial distribution of chemical elements in the samples was set randomly. The fraction of each element assumes values of 10, 20 or 30%. The samples had the shape of a cube having a side of 10 parameters of the fcc lattice. The edges were oriented in the <100> directions, and along them periodic boundary conditions were used. The temperature of the samples was 300 K, and the pressure was zero. The integration step for the MD calculations was 0.1 fs. After each 80 Monte Carlo steps, a calculation of 20000 MD steps was made. The calculations were stopped as soon as the energy of the system ceased to decrease by more than 0.01% of the initial value, which corresponds to ~ 0.004 eV/atom. Young's modulus was calculated during the tension of the samples along one of the <100> directions with a rate of 10^9 s^{-1}. Along the other two directions, the sample dimensions were changed so that the respective stress components were equal to zero.

For a detailed study of the atomic mechanisms of plastic deformation, we selected the stoichiometric compositions $Co_{10}Cr_{10}Fe_{30}Mn_{30}Ni_{20}$ and $Co_{30}Cr_{30}Fe_{10}Mn_{10}Ni_{20}$ having Young's moduli of 81 GPa and 103 GPa, respectively. The samples of such compositions will be further referred to as the $Fe_{30}Mn_{30}$-sample and the $Co_{30}Cr_{30}$-sample, respectively. In

addition, an equiatomic HEA and a Ni sample were examined. We generated 5 samples of each composition, with different initial element distributions for each composition. All of the crystallites had sizes of $10 \times 10 \times 10$ nm, and their edges were oriented along the directions [110], [$\bar{1}$10] and [001]. Tension and compression were performed along the [110] direction. The rest of the conditions coincided with those described above.

Identification of the local type of the crystal lattice was conducted on the basis of the algorithm determining the symmetry of the nearest-neighbor environment of each atom — Common Neighbor Analysis (CNA) [23]. According to the CNA, an intrinsic stacking fault (SF) in the fcc lattice is defined as two layers of atoms with an hcp symmetry of the nearest-neighbor environment.

3. Simulation results

The mechanical response of crystallites differs significantly for the considered stoichiometric compositions, loading types and rates. Primarily, this is manifested in the stress values σ and the fraction of atoms with a nearest-neighbor symmetry different from the fcc lattice. These quantities versus strain ε are shown in Fig. 1. The curves $\sigma(\varepsilon)$ deviate from a linear dependence at a strain of about 0.01 – 0.02, which is related to the growth of the fraction of atoms with bcc and undefined symmetries of the nearest-neighbor environment (Fig. 1). These rearrangements involve, to a greater extent, the atoms of Fe, Mn and Ni in the $Co_{30}Cr_{30}$-sample, and the Cr atoms in the $Fe_{30}Mn_{30}$-sample. They take place not in separately located atoms, but in such regions where the local fraction of atoms of this type is above their average fraction in the whole sample. As the elastic limit is reached, it is in these regions partial dislocations and intrinsic SFs nucleate, i.e. the fraction of atoms with an hcp symmetry of the nearest-neighbor environment increases. A decrease in $\dot{\varepsilon}$ from 10^9 to 5×10^8 s^{-1} can considerably change the structural response of crystallites. As $\dot{\varepsilon}$ further decreases to 10^8 s^{-1}, it does not change qualitatively.

3.1. Tension

For the $Fe_{30}Mn_{30}$-sample, depending on a specific distribution of chemical elements in the sample, either one SF may nucleate, transforming into a twin at $\dot{\varepsilon} = 10^8 - 10^9$ s^{-1}, or simultaneously two SFs may nucleate in the non-parallel planes (111) and ($\bar{1}\bar{1}$1) at $\dot{\varepsilon} = 10^9$ s^{-1}. The σ–ε curve for the first case is displayed in Fig. 1a, and the structure of the $Fe_{30}Mn_{30}$-sample is shown in Fig. S1 (supplementary material). Upon the first stress unloading at $\varepsilon = 0.068$, the SF intersects itself through the sample's periodic boundaries, but only in one plane — (111) (Fig. S1a, b). After that, the quantity of the hcp atoms does not change. Under further loading, σ grows significantly and falls at $\varepsilon = 0.096$: an extrinsic SF has started to grow (Fig. S1c). When dislocations meet again at $\varepsilon = 0.14$, σ starts to grow again (Fig. S1d). At $\varepsilon = 0.156$ dislocations start to move and a twin forms with a thickness of 4 atomic layers (Fig. S1e). The σ–ε curves and faults have a similar behavior in the case of the $Fe_{30}Mn_{30}$-sample at $\dot{\varepsilon} = 10^9$ s^{-1} and in the case of the $Co_{30}Cr_{30}$-sample at $\dot{\varepsilon} = 10^8$ s^{-1}.

At $\dot{\varepsilon} = 10^9$ s^{-1}, a single SF did not nucleate in any of the 5 calculations for the $Co_{30}Cr_{30}$-sample. This is related to the fact that in that sample the elastic limit stresses are more than twice higher than in the $Fe_{30}Mn_{30}$-sample and are sufficient for the nucleation of plasticity in two planes at once — (111) and ($\bar{1}\bar{1}$1). A description of the structural rearrangements taking place at $\dot{\varepsilon} = 10^9$ s^{-1} in the $Fe_{30}Mn_{30}$-sample and the $Co_{30}Cr_{30}$-sample, where not a single SF, but several SFs nucleate at once, is given in the supplementary material (Figs. S2 – S5).

3.2. Compression

In contrast to tension, the variation of $\dot{\varepsilon}$ under compression does not lead to any considerable differences in the system of defects.

As the elastic limit is reached in the $Fe_{30}Mn_{30}$-sample (Fig. 1b), alternating layers with bcc and undefined structures form. SFs nucleate in them, and after intersection the SFs form bands with an hcp lattice, their thickness being 3 – 4 atomic planes (Fig. S6a). Due to shears in the (111) bands (Fig. S6b) a substantial drop in σ occurs. Further motion of dislocations starts in all the hcp bands and leads to a decrease in their length and thickness (Fig. S6c) — the quantity of hcp atoms decreases and σ declines significantly (Fig. 1b). At $\varepsilon = 0.15$ the hcp bands transform into SFs, whereas in a range of $\varepsilon = 0.18 - 0.20$ a system of SFs forms in the sample in the ($\bar{1}\bar{1}$1) planes. A description of the response of the $Fe_{30}Mn_{30}$-sample at $\dot{\varepsilon} = 10^9$ s^{-1} is given in the supplementary material (Figs. S7, 8).

During the compression of the Co30Cr30-sample at $\dot{\varepsilon} = 10^8$ s^{-1}, as the elastic limit is reached, σ decreases almost 4-fold and then practically does not vary with increasing strain (Fig. 1c). By $\varepsilon = 0.09$ there has formed a small rhomb-shaped region of intersection of SFs and hcp bands, which borders with a single (111) SF, intersecting the whole sample (Fig. S9b). By $\varepsilon = 0.105$ this SF has split in two, and by $\varepsilon = 0.117$ these SFs have disappeared (Fig. S9c, d). The further structural response of the sample is determined by the alternating emission and absorption of SFs in the ($\bar{1}\bar{1}$1) and (111) planes (Fig. S9e – i). Corresponding to this are the growth and fall regions of the curve showing the quantity of the hcp atoms in Fig. 1c. As $\dot{\varepsilon}$ is increased to 10^9 s^{-1}, no significant differences from the response at $\dot{\varepsilon} = 10^8$ s^{-1} are observed for the $Co_{30}Cr_{30}$-sample (Figs. S10, 11).

4. Discussion

The differences in the response of the samples subjected to deformation are related to the following. Calculations made for small samples with different stoichiometric compositions show that an increase in the fraction of Co and Ni and a respective decrease in the fraction of Cr, Fe and Mn leads to an increase in the Young's modulus of the alloy. This is in agreement with the paper [9] where the effect of the solid-solution strengthening of the $Co_xFe_{50-x}Cr_{25}Ni_{25}$ HEA with Co with decreasing Fe content was discovered. The total fraction of Co, Ni and Cr is the same in both samples, while the content of Fe and Mn is 20% higher in the $Fe_{30}Mn_{30}$-sample, therefore it has a lower strength. The fact that the structural

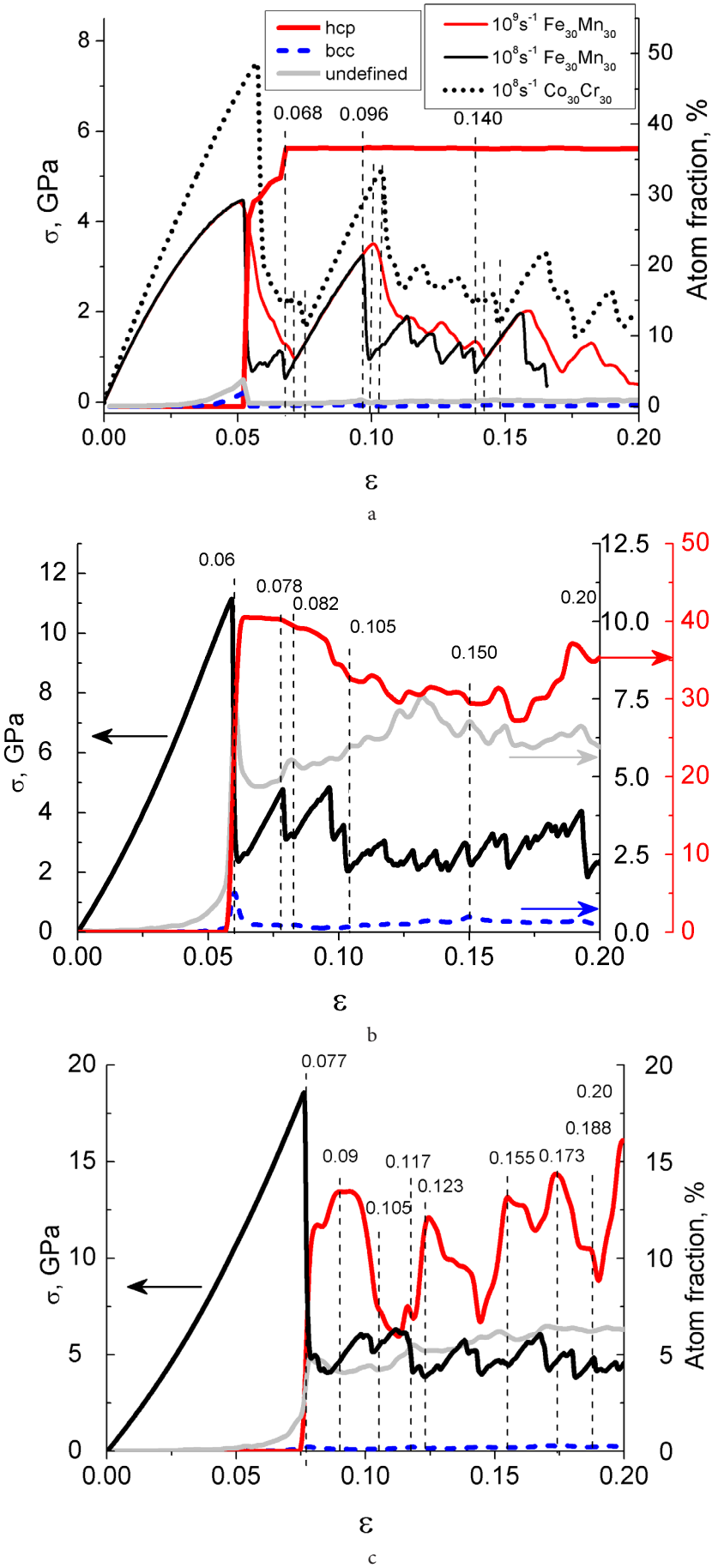

Fig. 1. Stress along the [110] direction (left axes) and the fraction of bcc, hcp and undefined atoms versus strain (right axes) for the tension of the $Fe_{30}Mn_{30}$-sample and the $Co_{30}Cr_{30}$-sample (a) and for the compression of the $Fe_{30}Mn_{30}$-sample and the $Co_{30}Cr_{30}$-sample (b,c) for different values of $\dot{\varepsilon}$.

rearrangements governing the nucleation of SFs involve primarily the atoms of Fe, Mn and Ni in the $Co_{30}Cr_{30}$-sample and the Cr atoms in the $Fe_{30}Mn_{30}$-sample, is accounted for by a stronger interaction of atoms in the $Co_{30}Cr_{30}$-sample in the pairs Co-Fe, Ni-Mn and Ni-Fe than in the others. In the $Fe_{30}Mn_{30}$-sample the strongest interaction is between the Cr atoms. This is reflected in the fact that the first peaks of the radial distribution functions for these pairs are much higher than the first peaks for the other pairs of elements, see Fig. S12 (supplementary material).

Since $\dot{\varepsilon}$ in the MD calculations is much higher than the experimental rates of tension/compression, the obtained results are in good agreement with the experiments and simulation of the shock loading of metals [24]. They note a high density of SFs and twins in nickel after the passing of a shock wave. The comparison of the data from the loading of the HEA and Ni in that paper does not reveal any significant differences, except for the fact that the nucleation of plasticity in the HEA occurs sooner, which is related to a strong distortion of the lattice due to the multiplicity of components of the HEA [21]. In addition, during compression the quantity and area of SFs is much smaller in Ni than in the HEA samples, which is associated with its high SF energy.

The obtained results are also in agreement with the data from the low-rate loading of the HEA, but in their comparison it is necessary to take into account the high-strain-rate character of plasticity in the simulated material. The formation of wide bands with an hcp lattice is related to the fact that the potential shows a higher stability of the hcp phase as compared to the fcc one. This was also established for the equiatomic alloy in MD [21] and *ab-initio* calculations [25]. In the paper [14] it was demonstrated that the SFs in the $Fe_{49.5}Mn_{30}Co_{10}Cr_{10}C_{0.5}$ alloy are the nucleation sites of the hcp phase whose fraction reaches 36% at the stage of necking during tension. In the FeCoCrMnC alloy the fcc-hcp phase transition was also revealed [26].

The response of the equiatomic sample to tension is similar to the response of the $Fe_{30}Mn_{30}$-sample at the examined $\dot{\varepsilon}$ (Figs. S13, 14) because the equiatomic sample and the $Fe_{30}Mn_{30}$-sample have similar Young's moduli (81 and 86 GPa) which are lower than that of the $Co_{30}Cr_{30}$-sample (103 GPa). The response of the equiatomic sample to compression is closer to that of the $Co_{30}Cr_{30}$-sample (Figs. S15, 16), since they both have high bulk moduli (183 and 239 GPa), while the $Fe_{30}Mn_{30}$-sample has one of the lowest bulk moduli (160 GPa). The results of the loading simulation of the equiatomic sample correspond qualitatively to the results of the quasi-static tension of the equiatomic alloy nanowire at 0 K reported in [21]: first, intrinsic SFs nucleate and grow, then twinning takes place. The quantitative differences are conditioned by the zero temperature and the presence of the free surface of the sample in [21], which promote twinning. The simulation results are also confirmed by the experimental and theoretical studies [27] where a single crystal of the equiatomic alloy is compressed along the $[5\bar{9}1]$ direction. The primary shear took place in the same {111} planes, but by means of the 1/2<110> dislocations, then twinning occurred in the sample. This difference in the type of dislocations is associated with the orientation of the samples with respect to the loading direction and the presence of free surface.

5. Conclusion

Irrespective of the stoichiometric composition, during the high-rate compression or tension the plasticity in the single crystals of the CoCrFeMnNi HEA nucleates through the formation of intrinsic SFs. Their generation is preceded by fcc-bcc-hcp local structural rearrangements in the vicinity of the atoms of Fe, Mn, Ni or Cr in the $Co_{30}Cr_{30}$-sample or the $Fe_{30}Mn_{30}$-sample, respectively. This is related to the strongest interaction between the mentioned elements, which follows from the corresponding radial distribution functions.

It has been shown that the structural and mechanical response of the alloys during deformation is to a large extent determined by their stoichiometric composition, loading type and rate. In the examined HEAs, twinning occurs during tension after the formation of a network of intersecting SFs and bands with an hcp lattice. It is not observed during compression. The elastic limit stresses of the $Co_{30}Cr_{30}$-sample during tension and compression are more than twice higher than the respective values for the $Fe_{30}Mn_{30}$-sample. SFs and the hcp phase layers in the $Fe_{30}Mn_{30}$-sample nucleate and grow more intensively than in the $Co_{30}Cr_{30}$-sample.

It has been shown that as the loading rate $\dot{\varepsilon}$ decreases from 5×10^8 s^{-1} to 10^8 s^{-1}, the material's response stops varying. During tension at $\dot{\varepsilon}=10^8$ s^{-1} in the HEA a SF nucleates, then transforming into a twin. This may take place also at 10^9 s^{-1} in the $Fe_{30}Mn_{30}$-sample and in the equiatomic sample. A totally different defect structure forms during tension at $\dot{\varepsilon}=10^9$ s^{-1}: several intersecting SFs nucleate. Further loading leads to the fragmentation of the $Fe_{30}Mn_{30}$-sample with the formation of grain boundaries perpendicular to the tension direction. In the $Co_{30}Cr_{30}$-sample there forms a twin intersecting the SFs lying transversely. The response of the $Co_{30}Cr_{30}$-sample during compression practically does not depend on $\dot{\varepsilon}$: there form regions of intersection of SFs which alternately emit and absorb SFs. In the $Fe_{30}Mn_{30}$-sample during compression at $\dot{\varepsilon}=10^8-10^9$ s^{-1} there forms a system of intersecting hcp bands. At 10^8 s^{-1} they transform into SFs and remain in the parallel planes. At 10^9 s^{-1} in the sites of bands intersection there form hcp regions with an unfavorable orientation for slip, and they become disordered in the process of loading.

The differences in the response of the samples are related to the fact that the variation of the fraction of each element has a different effect on the physico-mechanical properties of HEAs. An increase in the fraction of Co and Ni and a respective decrease in the fraction of Cr, Fe and Mn leads to an increase in the Young's modulus of the alloy. The fraction of Ni and the ratio between the fractions of Co and Cr are the same in both samples and they do not change the modulus, whereas the content of Fe and Mn is 20% higher in the $Fe_{30}Mn_{30}$-sample, therefore it has a lower strength. In addition, both Co and Cr increase the alloy's bulk modulus.

The results from the loading of HEAs and Ni do not differ qualitatively, which indicates the common deformation mechanisms of multi-component fcc HEAs and metals. The response of the equiatomic sample during tension and compression is similar to the response of the $Fe_{30}Mn_{30}$-sample and the $Co_{30}Cr_{30}$-sample, respectively, due to its close values

of Young's modulus and bulk modulus to the values of the $Fe_{30}Mn_{30}$-sample and the $Co_{30}Cr_{30}$-sample, respectively.

The presented simulation results from the high-rate loading of HEAs and Ni are in agreement with the shock loading calculations and experiments, as well as low-rate deformation, and expose the atomic mechanisms of plasticity of HEAs.

Acknowledgements. The work was carried out with the financial support of the Russian Science Foundation (project No. 17-79-10108).

Supplementary Material. *The on-line version of this paper contains supplementary material (figures) available free of charge at the journal's Web site (www.lettersonmaterials.com).*

References

1. D. B. Miracle, O. N. Senkov. Acta Mater. 122, 448 (2017). DOI: 10.1016/j.actamat.2016
2. B. Gludovatz, A. Hohenwarter, D. Catoor, E. H. Chang, E. P. George, R. O. Ritchie. Science. 345(6201), 1153 (2014). DOI: 10.1126/science.1254581
3. T. Fujieda, H. Shiratori, K. Kuwabara, M. Hirota, T. Kato, K. Yamanaka, Yu. Koizumi, A. Chiba, S. Watanabe. Mater. Lett. 189, 148 (2017). DOI: 10.1016/j.matlet.2016.11.026
4. S. Guo. Mater. Sci. Technol. 31(10), 1223 (2015). DOI: 10.1179/1743284715Y.0000000018
5. K. G. Pradeep, C. C. Tasan, M. J. Yao, Y. Deng, H. Springer, D. Raabe. Mater. Sci. Eng. A. 648, 183 (2015). DOI: 10.1016/j.msea.2015.09.010
6. D. Miracle, B. Majumdar, K. Wertz, S. Gorsse. Scripta Mater. 127, 195 (2017). DOI: 10.1016/j.scriptamat.2016.08.001
7. O. N. Senkov, J. D. Miller, D. B. Miracle, C. Woodward. Calphad. 50, 32 (2015). DOI: 10.1016/j.calphad.2015.04.009
8. H. Y. Diao, R. Feng, K. A. Dahmen, P. K. Liaw. Curr. Opin. Solid State Mater. Sci. 21(5), 252 (2017). DOI: 10.1016/j.cossms.2017.08.003
9. W. Fang, R. Chang, X. Zhang, P. Ji, X. Wang, B. Liu, J. Li, X. He, X. Qu, F. Yin. Mater. Sci. Eng. A. 723, 221 (2018). DOI: 10.1016/J.MSEA.2018.01.029
10. I. Toda-Caraballo. Scripta Mater. 127, 113 (2017). DOI: 10.1016/J.SCRIPTAMAT.2016.09.009
11. J. Li, Q. Fang, B. Liu, Y. W. Liu, Y. Liu. RSC Adv. 6(80), 76409 (2016). DOI: 10.1039/C6RA16503F
12. A. Sharma, P. Singh, D. D. Johnson, P. K. Liaw, G. Balasubramanian. Sci. Rep. 6, 31028 (2016). DOI: 10.1038/srep31028
13. B. Schuh, F. Mendez-Martin, B. Völker, E. George, H. Clemens, R. Pippan, A. Hohenwarter. Acta Mater. 96, 258 (2015). DOI: 10.1016/J.ACTAMAT.2015.06.025
14. Z. Li, C. C. Tasan, H. Springer, B. Gault, D. Raabe. Sci. Rep. 7, 40704 (2017). DOI: 10.1038/srep40704
15. J. Y. Ko, S. I. Hong. J. Alloys Compd. 743, 115 (2018). DOI: 10.1016/j.jallcom.2018.01.348
16. I. F. Golovnev, E. I. Golovneva, L. A. Merzhievsky, V. M. Fomin. Phys. Mesomech. 16(4), 294 (2013). DOI: 10.1134/S1029959913040036
17. S. V. Dmitriev, M. P. Kashchenko, J. A. Baimova, R. I. Babicheva, D. V. Gunderov, V. G. Pushin. Letters on materials. 7(4), 442 (2017). (in Russian) [С. В. Дмитриев, М. П. Кащенко, Ю. А. Баимова, Р. И. Бабичева, Д. В. Гундеров, В. Г. Пушин. Письма о материалах. 7(4), 442 (2017).] DOI: 10.22226/2410-3535-2017-4-442-446
18. S. Plimpton. J. Comput. Phys. 117(1), 1 (1995). DOI: 10.1006/jcph.1995.1039
19. W.-M. Choi, Y. Kim, D. Seol, B.-J. Lee. Comput. Mater. Sci. 130, 121 (2017). DOI: 10.1016/j.commatsci.2017.01.002
20. C. Wu, B.-J. Lee, X. Su. Calphad. 57, 98 (2017). DOI: 10.1016/j.calphad.2017.03.007
21. W.-M. Choi, Y. H. Jo, S. S. Sohn, S. Lee, B.-J. Lee. npj Comput. Mater. 4(1), 1 (2018). DOI: 10.1038/s41524-017-0060-9
22. B. Sadigh, P. Erhart, A. Stukowski, A. Caro, E. Martinez, L. Zepeda-Ruiz Phys. Rev. B. 85(18), 184203 (2012). DOI: 10.1103/PhysRevB.85.184203
23. J. D. Honeycutt, H. C. Andersen. J. Phys. Chem. 91(19), 4950 (1987). DOI: 10.1021/j100303a014
24. H. N. Jarmakani, E. M. Bringa, P. Erhart, B. A. Remington, Y. M. Wang, N. Q. Vo, M. A. Meyers. Acta Mater. 56(19), 5584 (2008). DOI: 10.1016/j.actamat.2008.07.052
25. Z. Li, F. Körmann, B. Grabowski, J. Neugebauer, D. Raabe. Acta Mater. 136, 262 (2017). DOI: 10.1016/j.actamat.2017.07.023
26. Z. Li, D. Raabe. Mater. Chem. Phys. 210, 29 (2018). DOI: 10.1016/j.matchemphys.2017.04.050
27. L. Patriarca, A. Ojha, H. Sehitoglu, Y. I. Chumlyakov. Scripta Mater. 112, 54 (2016). DOI: 10.1016/J.SCRIPTAMAT.2015.09.009